International Journal of Plasticity 186 (2025) 104246

Contents lists available at ScienceDirect

International Journal of Plasticity

journal homepage: www.elsevier.com/locate/ijplas

3D interface size effects on slip transfer in Ti/Nb nanolaminates

Nicolas Fuchs-Lynch [a,*], Mauricio De Leo [b], Pulkit Garg [a], Shuozhi Xu [c], Nathan A. Mara [b], Irene J. Beyerlein [a,d]

[a] Materials Department, University of California, Santa Barbara, 93106-5050, CA, USA
[b] Department of Chemical Engineering and Materials Science, University of Minnesota Twin Cities, Minneapolis, 55455, MN, USA
[c] School of Aerospace and Mechanical Engineering, University of Oklahoma, Norman, 73109, OK, USA
[d] Department of Mechanical Engineering, University of California Santa Barbara, Santa Barbara, 93106-5050, CA, USA

ARTICLE INFO

Keywords:
Nanolaminates
Interfaces
Dislocations
Stacking faults
Phase field modeling

ABSTRACT

Two-phase nanolaminates are well-renowned for achieving extraordinarily high strengths but at the sacrifice of reduced toughness and strain to failure. Recently "thick" interfaces, or so called 3D interfaces, in Cu/Nb nanolaminates were experimentally shown to improve both of these mechanical properties. In this work, we study the effect of 3D interfaces in the hexagonal close packed (HCP)/body centered cubic (BCC) Ti/Nb nanolaminate system. Nanoindentation hardness testing suggests increased strength with the introduction of a 3D Ti–Nb interface and a positive size effect with increases in 3D interface thickness from 5 nm to 20 nm. To understand this effect from a single dislocation perspective, we present a phase-field dislocation dynamics (PFDD) model for multi-phase HCP/BCC systems. We employ the model to simulate stress-driven transfer of single dislocations across 3D Ti/Nb interfaces of various thicknesses. Our results show that the critical stress for slip transfer increases with the thickness of the interface. This positive size effect is stronger for transfer from basal or prismatic dislocations in the Ti layer to $110\langle 111\rangle$ dislocations in the Nb layer than the reverse. For this Ti/Nb system, a critical thickness of 2 nm is identified at which the asymmetry in slip transfer is minimized. This work showcases 3D interfaces as a beneficial microstructure modification to strengthen as well as reduce anisotropy in nanocrystalline materials containing HCP phases.

1. Introduction

Two-phase metal nanolaminates have been extensively studied over the past couple of decades due to their extraordinarily high strength and stability with respect to extreme conditions, like high temperatures, irradiation, and high-rate impact (Zheng et al., 2014; Nasim et al., 2020; Beyerlein et al., 2022; Nizolek et al., 2016; Wu et al., 2023; Liang et al., 2024). These nanolaminates consist of alternating layers of two different metals. The thickness of the individual layers range from two to several tens of nanometers and often only a single grain spans the layer thickness. Consequently, all gliding dislocations must interact with the biphase interfaces due to the fine nanometer interface spacing (Beyerlein et al., 2015), and dislocation transfer across the biphase interface controls the strength of the composite (Misra et al., 2002).

Early studies concerning dislocation transfer across a bimetal interface examined differences in the properties of the adjoining phases, such as their elastic properties, stacking fault energies, crystallographic orientation, and lattice structure (Hunter et al., 2018; Mayeur et al., 2015; Koehler, 1970; Hirsch and Kelly, 1965). Marked contrast between any of these properties have been suggested

* Corresponding author.
E-mail address: nfuchs-lynch@ucsb.edu (N. Fuchs-Lynch).

https://doi.org/10.1016/j.ijplas.2025.104246
Received 31 October 2024; Received in revised form 3 January 2025
Available online 20 January 2025

to enhance the critical stress for slip transfer (Hunter et al., 2018). More recent work further considered the role of the structure of the interface itself on the slip transfer process (Mara et al., 2010; Mara and Beyerlein, 2014; Yu-Zhang et al., 2008; Martínez et al., 2014; Jian et al., 2021). A chemically sharp interface can span from 0.5 to 1.0 nm in thickness, and consists of one or two planes contributed by each adjoining phase. The atomic coordination of these interface planes differs from that of the parent phase and can be described by a discrete misfit dislocation network and/or facets (Chen et al., 2017; Misra et al., 2002; Beyerlein and Wang, 2019; Demkowicz et al., 2008; Wang et al., 2014).

Very recently, the concept of a "3D interface" (3DI) was introduced and demonstrated to improve both nanolaminate strength and strain to failure compared to its nearly atomically sharp counterpart (Chen et al., 2020a; Cheng et al., 2022). In the 3DI, changes in structure and composition from one layer to the next occur over several tens of atomic planes. Conventional or sharp interfaces are usually only two or a few atomic planes thick and are referred to hereafter as "2D interfaces" (2DIs). Consequently, the misfit strains between the adjacent pure crystals are spread over the thickness of the 3DI, consisting of smooth or abrupt changes in chemistry and/or crystal structure. Bearing a noticeable thickness, the 3DI can be viewed as a class of interphase, potentially differing in composition and structure than either phase it joins. However the 3DI does not contain elements that are not already in the nanolaminate and thus, the 3DI does not alter the overall chemical composition of the nanolaminate. The attributes unique to 3DIs, such as its thickness, crystal structure, and composition, and their role in the interfacial slip transfer process are at the heart of this investigation. These parameters, particularly the 3DI thickness, were investigated based on their importance in previous studies regarding 3DIs. In the Cu/Nb 3DI system, when the 3DI thickness was the same as the pure layer thickness, the strength and elongation to failure were improved relative to the case with a much larger pure layer thickness (Cheng et al., 2022). This size effect was proposed to occur as a result of the 3DI hindering dislocation pileups from gliding across the interface. The effect of the 3DI was seen to be more significant when the pure layer thickness was lower, as this limited the maximum pileup size that could develop in a pure layer. This size effect should be present in Ti/Nb 3DIs since the same argument for pileups is independent of the system. The 3D interface and pure layer thickness can be optimized, which is beneficial for mechanical performance.

Up to now, studies on crystalline nanolaminates containing 3DIs have been limited to the face centered cubic (FCC)/body centered cubic (BCC) Cu/Nb system. Some interesting distinctions can result from nanolaminate systems possessing even greater mechanical contrast, such as hexagonal close-packed (HCP)/BCC systems (Beyerlein and Wang, 2019; Carpenter et al., 2015a; Pathak et al., 2017; Jain et al., 2023). HCP metals can bear many desirable structural properties, such as favorable strength-to-weight ratio, high temperature stability, radiation resistance, and biocompatibility compared to cubic metals (Hasirci and Hasirci, 2018; Graff, 2008; Campbell et al., 1961; Woo, 2000). HCP metals exhibit a more complex deformation behavior as they tend to be more elastically and plastically anisotropic and deform by multiple slip modes. Nevertheless, not only do HCP/BCC nanolaminates with 3DIs provide potentially new applications but can produce new insight into anisotropy effects in slip transfer processes. Given that features such as grain boundary complexions (Khalajhedayati and Rupert, 2015; Cantwell et al., 2020) share many of the characteristics of 3DIs, this work also has implications spanning both crystalline and amorphous nanomaterials.

In this work, we study the effect of the thickness of the 3DI in Ti/Nb nanolaminates. Magnetron sputtering is employed to synthesize a range of nanostructured Ti–Nb materials. Characterization and nanoindendation tests show increases in hardness with the introduction of a 3DI and with increasing 3DI thickness. At a finer scale, via computation, we simulate the transfer of dislocation slip across 2D and 3DIs of varying thicknesses. To this end, a mesoscale phase field dislocation dynamics (PFDD) model is developed to treat dislocation dynamics in a two-phase HCP/BCC nanolayered system. The formulation takes into account the differences in stacking fault energies, elastic anisotropy, crystal structure, and lattice parameter for both HCP and BCC phases. The PFDD simulations reveal that the critical stress for complete slip transfer across the 3DI increases as the 3DI thickness increases to approximately 5–10 nm and plateaus thereafter. The analysis suggests a path dependence, with the potential to increase glide resistance by an order of magnitude when transferring from Ti to Nb, but only 12% in the reverse direction. Notably, a fine 3D Ti–Nb layer of 2 nm removes the orientation dependence between the two pathways, which has positive implications for co-deformation. Furthermore, the simulation results imply that thicker interfaces are stronger only up to a certain thickness, of around 10 nm.

The paper is structured as follows. We begin with a review of prior slip transfer models. Next, we describe methods for synthesis, characterization and nanomechanical testing on thin films of Ti/Nb nanolaminates as well as reference nanostructured materials. We then present the extension to the PFDD model to treat multiple crystal structures where one is cubic and another HCP. We follow with the material input, DFT calculations for the Ti–Nb binary and simulation setup. Experimental and modeling results on 3DI size effects are then presented. We end with discussion on the important role of interface stacking fault energy on transfer path dependence.

1.1. Modeling background on slip transfer in 2D and 3DIs

Slip transfer across a crystalline interface has been treated by a variety of modeling techniques: analytical dislocation theory, atomistic simulation, and mesoscale dislocation models (Hunter et al., 2018; Bormann et al., 2019; Xu et al., 2022c; Albiez et al., 2019). Most analytical models take into account one effect, either the image forces due to moduli mismatch or the misfit strain field due to the lattice mismatch or the penalty of forming a residual dislocation in the interface (Hunter et al., 2018). Koehler (Koehler, 1970) focused on the moduli mismatch and forecasts the critical stress for transmitting a screw dislocation starting in the softer of the two materials:

$$\tau_{crit} \approx \frac{(\mu^{(2)} - \mu^{(1)})\mu^{(1)} b}{4\pi(\mu^{(2)} + \mu^{(1)})c'} \tag{1}$$

Here, $\mu^{(1)}$ and $\mu^{(2)}$ are the shear modulus in the donor and recipient materials, respectively, c' is the distance between the dislocation and the interface, and b is the Burgers vector magnitude. The model presumes that strengthening occurs only when the recipient material is stiffer than donor material and not the other way around. The greater the difference in moduli, the greater is the enhancement in strength. Another model by Hirsch and Kelly considers the difference in stacking fault energy between the two materials and poses that slip transfer resistance is enhanced only when moving from a material of lower to higher stacking fault energy (Hirsch and Kelly, 1965). This effect certainly needs to be considered when investigating slip transfer across 3DIs.

Several molecular dynamics (MD) studies have probed the connection between the mechanism of slip transfer and the properties which affect it (such as image forces, coherency stresses, or misfit dislocations) in biphase materials with various layered structures (Rao and Hazzledine, 2000; Wang and Misra, 2011). It was shown that coherency stresses can alter the Koehler stresses by changing the elastic constants locally at the interface, and cause Escaig stresses which can alter the core structure of the incoming dislocation (Rao and Hazzledine, 2000). It is likely that the structure of the 3DI will affect the slip transfer process. We elect to not use MD in this investigation given the high strain rates involved and limitations in simulation length scale relative to that of the layers.

Crystal plasticity based modeling has been used to investigate slip transfer across both grain boundaries (Acharya, 2007; Ashmawi and Zikry, 2002; Chen et al., 2020b; Haouala et al., 2020; Agius et al., 2022; Ahmadikia et al., 2021) and bimetal interfaces (Mayeur et al., 2015; Cheng et al., 2024). These models adopt criteria for slip transmission based on those presented by Lee–Roberston–Birnbaum (Lee et al., 1990), and can account for the change in the character of the interface throughout deformation. Capturing the effects of this coupling has been simulated for the Cu/Nb interface (Beyerlein and Mayeur, 2015), providing insights into the evolution of interfaces and grain structure as a result of plasticity. However, this larger length scale model does not take into account changes in stacking fault energy that accompany slip transfer and does not explicitly model individual dislocations, which we intend to study here.

Phase Field Dislocation Dynamics (PFDD) is the method we adopt for this investigation. This method can simulate the evolution of dislocation configurations and motion in crystals (Beyerlein and Hunter, 2016; Xu et al., 2020b). PFDD is adequately suited for this investigation as it takes into account the structural details at the dislocation core while being able to simulate larger length and longer time scales than atomistic methods. This means simulations of longer propagation trajectories for one or more dislocations. The basic atomic scale input can easily be obtained from DFT, which translates to a wider range of systems that can be considered in simulation, not just those with reliable interatomic potentials. A system energy containing the elastic energy, generalized stacking fault energy, gradient term and work done is minimized at every time step (Mianroodi and Svendsen, 2015; Roach et al., 2023) to predict the dislocation configuration. PFDD has been developed for a range of crystal structures, including HCP and BCC. For HCP metals, the stress-free equilibrium stacking fault widths (SFW) for the various dislocation types were shown to agree with reported values from DFT, MD, and experiment for Mg and Ti (Albrecht et al., 2020). For BCC metals, the edge/screw core structures, the linear elastic strain field outside the core, and the anisotropic expansion of a loop compared well with predictions from analytical models or MD (Fey et al., 2022). The PFDD formulation has been extended to treat heterogeneous systems, consisting of two or more materials with different elastic moduli (Lei et al., 2013; Xu et al., 2022b). The modification builds on the idea of an eigenstrain first introduced by Eshelby Eshelby (1957). With these recent advancements, PFDD has been used to study dislocation interactions with voids, shearable or non-shearable precipitates, and interfaces (Roach et al., 2023; Xu et al., 2022a). The multi-phase version has been applied to calculate the critical stresses associated with slip transfer across a range of 2D FCC/FCC interfaces, single phase Nb with a BCC CuNb alloy 3DI, and single phase Cu in an FCC CuNb alloy 3DI (Zeng et al., 2016; Xu et al., 2022c). In the case of the FCC/FCC interfaces, the simulations revealed that the critical slip transfer stress exhibited an asymmetry following:

$$\tau_{crit} \approx \frac{a^{(2)}\mu^{(2)}}{a^{(1)}+a^{(2)}}\left(\frac{a^{(1)}}{a^{(2)}}-\frac{\mu^{(1)}}{\mu^{(2)}}\right)^2 \tag{2}$$

where $a^{(1)}$ and $\mu^{(1)}$ are the lattice parameter and shear modulus for the material in which the dislocation originates and $a^{(2)}$ and $\mu^{(2)}$ for the material in which the dislocation transfers. The analytical model was remarkably predictive, even though it did not account for changes in the stacking fault energies or the degrees of cubic anisotropy between different materials. It would suggest that at least for 2D FCC/FCC interfaces, formation of the residual interface dislocation, coherency stress, and moduli mismatch are altogether dominant factors for slip transfer. In the FCC/FCC 3DI system, however, PFDD calculations demonstrated an effect of the relative stacking fault energies between the layer and 3DI on the slip transfer stress (Xu et al., 2022c). The slip transfer stress reached a maximum when the 3DI thickness h' and stacking fault width were similar. This result was predicted by an analytical model by Hirsch and Kelly, that did not account for the lattice parameter and elastic moduli mismatches across the interface (Hirsch and Kelly, 1965). It was also consistent with PFDD predictions for the bypass stress required for Ni dislocations interacting with a row of shearable precipitates (Zeng et al., 2019).

In this work, we employ the PFDD technique to simulate slip transfer across 3D interfaces in Ti/Nb nanolaminates. The model is formulated to determine dislocation motion in a system composed of multiple phases of different crystal structures, elastic moduli and levels of elastic anisotropy, namely one cubic (Nb) and one transversely isotropic (Ti). The only material properties needed for simulation are lattice constants, anisotropic elastic constants, and the generalized stacking fault energies (GSFE) for the relevant slip planes. The GSFE values are taken from DFT calculations, previously reported for pure Ti and Nb (Rodney et al., 2017; Albrecht et al., 2020; Xu et al., 2020a). Properties of the 3DI for the Ti–Nb binary, however, have not been previously determined and are calculated via DFT here. Simulations are carried out for two directions of slip transfer and two commonly observed HCP/BCC interface crystallographic characters. The analysis focuses on the effect of 3DI thickness on the critical slip transfer stress, its path dependence, and interface crystallography.

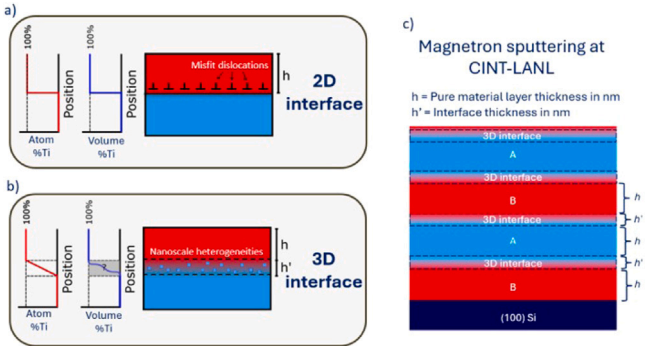

Fig. 1. (a) Conventional deposition method of a bimetal nanolaminate with atomically sharp interfaces. (b) Bimetal nanolaminate deposition containing 3DIs, in which the target power is gradually decreased to get a thick transition region between pure phases resulting in nanoscaled heterogeneities at the interface. (c) Overall microstructure schematic of the 3DI-containing nanolaminate.

2. Methods

2.1. Nanolaminate synthesis, morphological, and nanomechanical characterization

The experimental setup involved physical vapor deposition (PVD) of Ti/Nb thin film nanolaminates, composed of alternating pure layers of Ti and Nb of size h varying 3DI sizes of size h'. Two 6 μm 3D Ti/Nb nanolaminates were deposited of size $h = 20$ nm and $h' = 5$ nm, and size $h = 20$ nm and $h' = 20$ nm respectively. Additionally, as reference materials, a BCC Ti–Nb binary alloy and 20 nm nanocrystalline Ti thin films were deposited. The primary phases in the various samples were determined by 1D XRD, which can be seen in Supplementary Fig. 1. In order to rule out length scale effects contributing to the hardness measurements, the average grain size of the nanocrystalline Ti was found via a Scherrer grain size determination. The results of this can be seen in Supplementary Fig. 2. The precise length scales were determined through transmission electron microscopy and atom probe tomography (not shown).

All films were synthesized using DC Magnetron Sputtering PVD on Si (100) substrates with an amorphous native oxide layer. A schematic for this process can be seen in Fig. 1. The base pressure during deposition remained in the low 10^{-8} Torr range to minimize oxygen and contaminants. The target powers for Ti and Nb were set at 150 W and 130 W, respectively, with a throw distance of 12.7 cm, 6 rpm rotation, a surface bias of 20 W, and a working Ar pressure of 3 mTorr. The 3DIs were created by proportionally modulating the target powers, ramping down one target while ramping up the other over a specific period of time proportional to the desired h'.

The sample was prepared using focused ion beam (FIB) milling on an FEI Helios Dual Beam system. Initial cuts were made at 30 kV using a range of currents from 65 nA to 41 pA, followed by final polishing with a 1 kV, 0.22 nA cut. The finished TEM lamella was then transferred to a Thermo Fisher Talos F200X operating at 200 kV for morphological characterization. The Thermo Talos uses a Ceta CMOS camera for Conventional TEM and a Super-X G2 EDX detector for chemical profile acquisition. The chemical profiles were obtained from EDS patterns by integrating the signal through 10 nm of material perpendicular to the interface. The Atom Probe Tomography measurements were performed with a CAMECA local electron atom probe LEAP 4000X HR at 200 kHz pulse repetition rate, 0.5% detection rate, 30 K base temperature, and 30–60 pJ base energy. The APT data was reconstructed using CAMECA's integrated visualization software (IVAS) 6.3.

The nanomechanical data acquisition and analysis was performed using a Bruker Hysitron TI-890 equipped with a standard Berkovich diamond tip. Partial load-unload cycles ranging from 0.3 to 12 mN were performed to continuously measure hardness and reduced modulus within the top 400 nm of the film. The peak-to-valley surface roughness height varied from 20 to 40 nm. The area analyzed for the peak-to-valley surface roughness height is 10×10 μm initially and the indentation is conducted on a 3×3 μm subregion with ideal conditions. To avoid mechanical contribution from the substrate, the data collected comes from depths of 150 to 300 nm.

2.2. PFDD formulation

PFDD treats a discretized 3D system, where the free energy of every point is a function of scalar-valued order parameters which evolve in space and time. The order parameters ϕ^α represent the location of dislocation slip by dislocations in the slip system α. One order parameter is associated with slip by each slip system. An order parameter $\phi^\alpha = N$, represents a region that has been slipped by N times, whereas $\phi^\alpha = 0$ represents an unslipped region (Beyerlein and Hunter, 2016; Mianroodi and Svendsen, 2015).

For evolving the system, the total free energy is calculated at each timestep using the following contributions:

$$\psi(x) = \psi_{ela}(x) + \psi_{lat}(x) - \psi_{ext}(x) \tag{3}$$

In this equation, $\psi_{ela}(x)$ represents the elastic strain energy due to the dislocation and dislocation–dislocation interactions, $\psi_{ext}(x)$ is the work done by the dislocation under the applied stress, and $\psi_{lat}(x)$ accounts for the energy due to a dislocation moving through the lattice, where it breaks and re-forms atomic bonds. The inclusion and effect of the gradient term has been studied in prior works (Wang and Li, 2010; Xu et al., 2019; Mianroodi and Svendsen, 2015) It was shown that the gradient term coefficient affects the width of the partial cores and has second-order effects on the SFW. The coefficient can be used to achieve better fit with core structures from atomistic calculations (Roach et al., 2023). For simplicity, the gradient term is omitted in this work.

To define the elastic energy density, the eigenstrain tensor ϵ^0 is first defined as:

$$\boldsymbol{\epsilon}^0(x) = \begin{cases} \boldsymbol{\epsilon}^p(x) & x \in \text{material 1} \\ \boldsymbol{\epsilon}^p(x) + \boldsymbol{\epsilon}^v(x) & x \in \text{material N in regions where there are dislocations } (N \neq 1) \\ \boldsymbol{\epsilon}^v(x) & x \in \text{material N where there are not dislocations } (N \neq 1) \end{cases} \tag{4}$$

with $\boldsymbol{\epsilon}^v$ representing the virtual strain tensor, arising from the moduli mismatch.

The plastic strain tensor $\boldsymbol{\epsilon}^p$ is related to the plastic distortion tensor $\boldsymbol{\beta}^p$ and the order parameter ϕ_α as follows:

$$\boldsymbol{\epsilon}^p = sym\boldsymbol{\beta}^p \tag{5}$$

Above, sym represents the symmetric part of the tensor.

$$\boldsymbol{\beta}^p(\phi) = \sum_{n=1}^{n_{op}} \frac{b^\alpha \phi^\alpha}{d^\alpha}\, \boldsymbol{s}^\alpha \otimes \boldsymbol{n}^\alpha \tag{6}$$

Here, $\boldsymbol{s}^\alpha$ is the slip direction unit vector, b^α is the Burgers vector magnitude, $\boldsymbol{n}^\alpha$ is the slip plane normal, and d^α is the spacing between two adjacent slip planes for slip system α.

Next, $\psi_{ela}(x)$ can be represented accounting for the contributions of the homogeneous elastic energy density $\psi^{eq}_{ela}(x)$ and the additional elastic energy density $\psi^{ex}_{ela}(x)$, such that:

$$\psi_{ela}(x) = \psi^{eq}_{ela}(x) + \psi^{ex}_{ela}(x) \tag{7}$$

with

$$\psi^{eq}_{ela}(x) = \frac{1}{2}\,[\boldsymbol{\epsilon}(x) - \boldsymbol{\epsilon}^0(x)] \cdot \boldsymbol{C}[\boldsymbol{\epsilon}(x) - \boldsymbol{\epsilon}^0(x)] \tag{8}$$

$$\psi^{ex}_{ela}(x) = \frac{1}{2}\,\boldsymbol{\epsilon}^v(x) \cdot \boldsymbol{M}^{[N]}(x)\boldsymbol{\epsilon}^v(x) \tag{9}$$

In the above, $\boldsymbol{C}$ is the elasticity tensor, $\boldsymbol{\epsilon} = sym(\boldsymbol{\beta})$ is the strain tensor, $\boldsymbol{\beta} = \nabla \boldsymbol{u}$ is the distortion, and $\boldsymbol{u}$ is the displacement. For an arbitrary material $1 < N \leq N_{mat}$:

$$M^{[N]}_{ijkl}(x) = -C^{[1]}_{ijmn}[\Delta C^{[N]}_{mnpq}(x)]^{-1} C^{[1]}_{pqkl} - C^{[1]}_{ijkl} \tag{10}$$

$$\Delta C^{[N]}_{ijkl}(x) = C^{[N]}_{ijkl}(x) - C^{[1]}_{ijkl} \tag{11}$$

It is important to note that the virtual strain exists in all materials except for material 1.

The lattice energy density ψ_{lat} can be expressed as,

$$\psi_{lat}(x) = \frac{\gamma^{[N]}_{gsf}(\phi(x))}{l^{[N]}_{gsf}} \tag{12}$$

where $\gamma^{[N]}_{gsf}$ is the generalized stacking fault energy (GSFE) as a function of the order parameter ψ for material N and $l^{[N]}_{gsf}$ is the spacing between adjacent slip planes where the GSFE is calculated for material N.

The external energy density, ψ_{ext} can be expressed as follows:

$$\psi_{ext}(x) = \boldsymbol{\sigma}_{app}\boldsymbol{\epsilon}^0(x) \tag{13}$$

where $\boldsymbol{\sigma}_{app}$ represents the applied stress tensor.

At each timestep, the total system energy is minimized with respect to each order parameter ψ_α and the virtual strain components $\boldsymbol{\epsilon}_{ij}$ using the time-dependent Ginzburg–Landau (TDGL) equations, as follows:

$$\dot{\phi}^\alpha(x) = -m[\partial_{\phi_\alpha(x)}(\psi_{ela}(x) + \psi_{lat}(x) - \psi_{ext}(x))] \tag{14}$$

$$\dot{\epsilon}^v_{ij}(x) = -m^v \frac{\partial \psi}{\partial \epsilon^v_{ij}} \tag{15}$$

where m and m^v are relaxation coefficients. These constants are non-negative and control the rate of convergence to the equilibrium. Constant relaxation coefficients are selected so that a converged configuration and virtual strain are achieved in every time step. We find that setting them all to unity ensures convergence as the equilibrium state is independent of their values (Zeng et al., 2016).

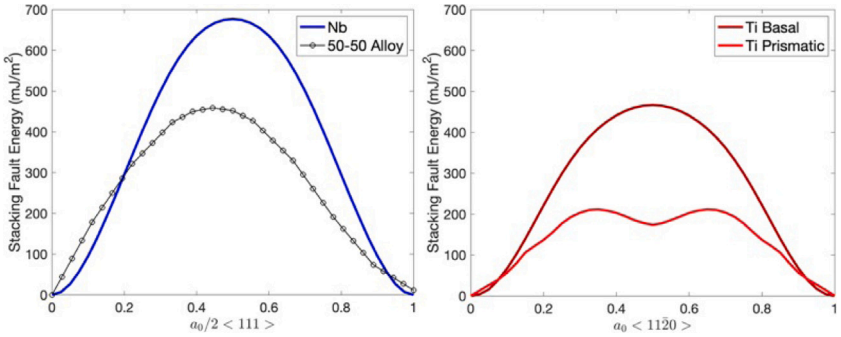

Fig. 2. GSFE curves for (a) Nb and the 50-50 BCC alloy and (b) Ti basal and Ti prismatic.

Table 1
Lattice parameters a_0 (in Å), elastic constants $C_{11}, C_{12}, C_{13}, C_{44}, C_{66}$ (in GPa), Isotropic shear modulus $\mu = \frac{3C_{44}+C_{11}-C_{12}}{5}$ (in GPa), μ_{dir} is the directional shear modulus in the glide plane, USFE (in mJ/m^2), and Burgers vector value (in Å).

Material/Plane	a_0	C_{11}	C_{12}	C_{13}	C_{44}	C_{66}	μ_{dir}	USFE	b
Nb/{110}	3.324	245.0	132.0	132.0	28.4	28.4	103.6	676.78	2.879
Ti/Basal	2.922	176.1	86.9	68.3	50.8	44.6	48.3	466.65	2.922
Ti/Prismatic	2.922	176.1	86.9	68.3	50.8	44.6	51.2	211.49	2.922
Interface/{110}	3.287	177.5	120.1	120.1	13.7	13.7	84.5	458.97	2.847

2.3. Material input

The model nanolaminate system is composed of three materials: HCP Ti, BCC Nb, and the 3DI. The interface is presumed to be a homogeneous solid solution binary Ti–Nb through its thickness. The stable crystal structure of this phase is BCC (Bönisch, 2016). In the PFDD formulation, Nb is assigned material $N = 1$, the Ti–Nb 3DI $N = 2$, and Ti $N = 3$.

For simplicity, the dislocations simulated here are assumed to be undissociated. The order parameter in Nb ϕ^1 and second one ϕ^2 in the 3DI correspond to shear on the $\{110\}\langle 111\rangle$ system and the third and fourth order parameters ϕ^3 and ϕ^4 are associated with either the basal $\{0001\}\langle 11\bar{2}0\rangle$ slip system or prismatic $\{10\bar{1}0\}\langle 11\bar{2}0\rangle$ slip system in Ti. The lattice energies in Nb and the alloy are associated with the $\{110\}$ GSFE curve and in Ti either the basal $\{0001\}$ curve or prismatic $\{10\bar{1}0\}$ GSFE curve.

For each material, PFDD utilizes the lattice parameter a_0, the full elastic tensor (C_{11}, C_{12}, and C_{44} for the BCC materials and $C_{11}, C_{12}, C_{13}, C_{44}$, and C_{66} for Ti), and the GSFE curve γ_{gsf}. Table 1 summarizes the constants and the USFE, which is the maximum of the GSFE curve. The elastic constants and lattice parameters for the pure materials are taken from experimental data at room temperature (Warlimont and Martienssen, 2018; Simmons, 1971). The GSFE curves for Nb and Ti are taken from prior DFT calculations (Rodney et al., 2017; Albrecht et al., 2020; Xu et al., 2020a)and are reproduced in Fig. 2.

2.4. DFT calculations for 50-50 BCC alloy

In order to calculate the elastic properties of the Ti–Nb 50/50 binary alloy BCC solid solution, DFT calculations using the Vienna Ab Initio Simulation Package (VASP) were performed. The generalized-gradient approximation (GGA) was used as was the Perdew–Burke–Ernzerhof (PBE) exchange–correlation functional (Perdew et al., 1996). For all calculations, Projector Augmented Wave (PAW) pseudopotentials were used, with a plane-wave cutoff energy of 550 eV. For the elastic constant calculation, a $2 \times 2 \times 2$ BCC supercell was used. It contained a total of 16 atoms in the form of a special quasi-random structure (SQS) generated with the alloy theoretic automated toolkit (ATAT) (Van De Walle et al., 2002). Its volume was relaxed via use of a Monkhorst–Pack k-point mesh of $9 \times 9 \times 9$. Atoms were relaxed at their respective positions by applying convergence criteria on the force and energy of 0.01 eV Å^{-1} and 10^{-5} eV, respectively. The elastic constants were calculated using the energy-strain method (Liu et al., 2005; Holec et al., 2012).

The BCC supercell for the GSFE calculation has dimensions of $2 \times 9 \times 2$ Å (with 72 atoms) along the [111], [110], and [112] directions. A 10 Å vacuum region was added in the [110] direction in order limit interactions between slip planes and the free surface. The top plane of the crystal was shifted along the [111] direction and then relaxed using a k-point mesh of $6 \times 1 \times 9$. Atoms were only allowed to relax along the slip plane normal direction.

2.5. Simulation setup

Fig. 3(a) shows the simulation set up. A simulation cell of a simplified geometry is designed to study the process of a dislocation in one material layer "phase A" to intersect an interface, transfer across it, and glide in the adjacent layer "phase B". The phases A and B are single crystals of either HCP Ti or BCC Nb. In between these phases is an interface of thickness h'. A 2D interface is

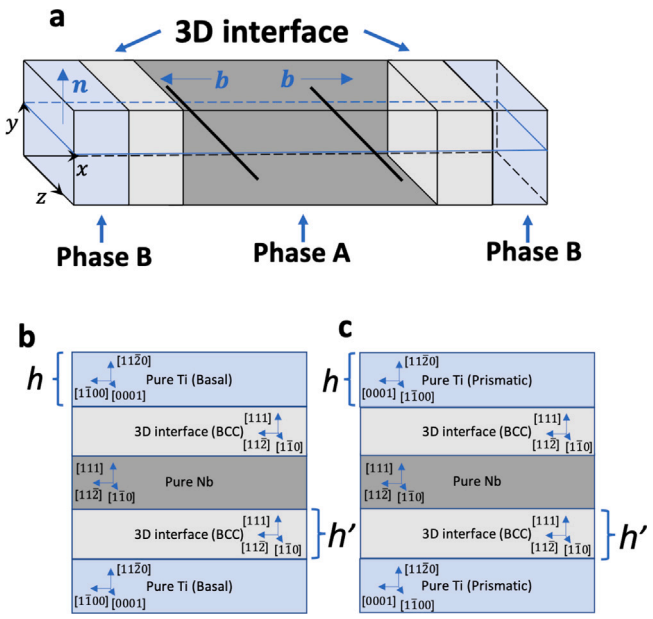

Fig. 3. (a) Simulation cell with dislocation dipole. Phase A or B is either Nb or Ti (basal or prismatic). (b-c) Schematic showing the respective crystallographic orientations of the 3DI throughout the simulation cell. (b) Case with Ti Basal. (c) Case with Ti Prismatic.

modeled by setting $h' = 1$ nm. Thicknesses of $h' = 2$ nm and greater are deemed 3DIs. We kept the volume fraction constant so that we could isolate the role of slip transfer across the 3D interfaces on material performance. When the 3D interface thickness is changed, so are the layer thicknesses. In this way, the contribution of the mechanical properties of the interface itself stays fixed.

The orientations of the crystals correspond to two predominant interface crystallographic characters which are perfectly aligned for slip transfer, shown in Fig. 3(b), (c). For the first orientation, denoted *Ti Prismatic*, the slip transfer pathway is a continuous one that connects the {110} plane in Nb and the 3DI and the $\{10\bar{1}0\}$ prismatic plane. The glide planes are aligned across the interface and there is no misorientation between them. The orientation of the BCC regions are ($[11\bar{2}]$, $[1\bar{1}0]$, [111]) and the HCP region is ([0001], $[1\bar{1}00]$, $[11\bar{2}0]$). For the second orientation, called *Ti Basal*, the pathway comprises the same plane in Nb and the 3DI and the {0001} basal plane. The crystallographic orientations of the BCC phases are the same but that for Ti changes to ($[1\bar{1}00]$, [0001], $[11\bar{2}0]$). As in the first orientation, the glide planes on either side of the boundaries are aligned.

When the dislocation transmits from material (1) to material (2), a residual dislocation is left behind at the interface. The Burgers vector is conserved during the transmission process so the residual Burgers vector is determined by $b^r = b^{(2)} - b^{(1)}$. In simulation, the formation of the residual dislocation in the interface causes a net displacement given by Zeng et al. (2016):

$$\boldsymbol{u}_r = \phi^{(2)}\boldsymbol{b}^{(2)} - \phi^{(1)}\boldsymbol{b}^{(1)} \tag{16}$$

Here, $\phi^{(i)}$ is the phase field variable at points along the interface plane contributed by material i.

Periodic boundary conditions are applied in all three directions. The FFT grid is a simple cubic grid. The grid spacing is $(\frac{\sqrt{3}a_0}{2}, \frac{\sqrt{2}a_0}{2}, \frac{\sqrt{6}a_0}{3})$. The simulation cell size in x depends on h', with the minimum x-dimension spanning 48 grid points and the maximum 832 grid points, corresponding to 1 nm and 20 nm thick 3DIs, respectively. In the y and z directions, 64 and 128 grid points were used for all simulations. Different values of y-dimension were tested to ensure that the values selected minimized Gibbs oscillations and effects of periodic images.

The simulations involve two steps. The first step is to insert an edge dislocation dipole and relax the system under zero stress. The dipole is placed in material A on the glide plane with its line direction parallel to the interface and Burgers vector normal to it. The position of the dipole is 1/4 and 3/4 of the simulation cell in the x direction and 1/2 of the simulation cell in the y direction. This spacing is sufficiently large that the dipole remains immobile under zero stress. In the next step, the simulation cell is subject to an applied shear stress, parallel to the glide plane and in the direction of slip. The shear stress is applied to the cell in fine increments to determine the minimum stress τ_c needed for the dislocation to transfer from material A, across the 3DI, and into material B. This stress needs to be sufficiently high such that after crossing the interface, the dislocation continues gliding in material B. The typical process usually involves finding a threshold stress at which the dislocation starts to move. While under constant stress, the dislocation can still arrest before fully transmitting to material B and requires an even higher applied stress to restart glide. The system equilibrates when the norm of the difference between the global vector of the order parameter and virtual strain is less than 10^{-4}.

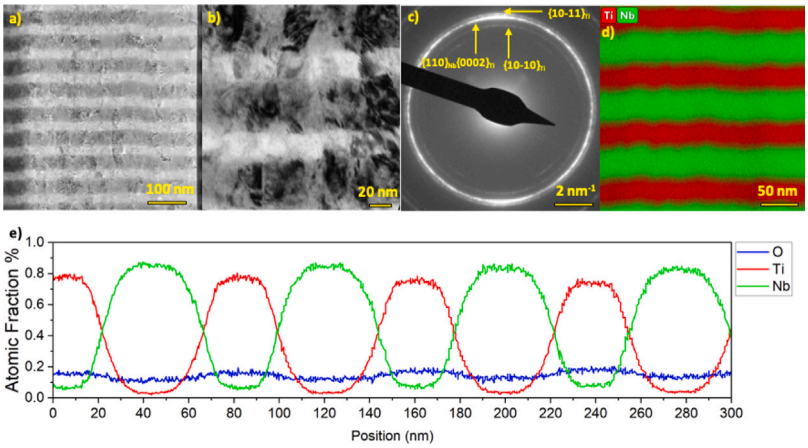

Fig. 4. (a) Bright-field (BF) CTEM micrograph of 3D h=20 h'=20 Ti/Nb with SADP. (b) Close-up of interfacial structure and sub-granular morphology under strong diffraction contrast due to introduction of a 10 um objective aperture in the center beam. (c) Close-up of primary diffraction rings in the SADP shown in (a). (d) STEM-EDS colormap showing chemically dissident layers and out-of-plane tortuosity of the interface. (e) Atomic fraction plot of integrated region shown in (d), showing the chemical proportion of each layer as a function of position.

3. Results

3.1. Morphological, chemical, and nanomechanical testing results

Characterization of the 3DI structure can be seen in Fig. 4. From the phase diagram, we would expect that the material is BCC. However, the SADP demonstrates consistent growth in the (110)//(0002) growth direction, verified by 2D-XRD (not shown). The diffraction rings in the SADP show well separated diffraction planes in HCP Ti, and an overlapped region of BCC Nb and HCP Ti and moderate texture from both materials. The EDS data shows the gradual transition and interfacial thickness between pure layers and allows for the determination of the 3DI thickness and the pure layer thickness. Since EDS displays a bidimensional representation of the interface, the atomic fraction as a function of position also has tortuosity effects convoluted into the interfacial thickness, which may cause variability to determine the real interfacial thickness. EDS simplifies the 3D morphology and its features. EDS averages the atoms in that pixel line parallel to the electron beam, so it fails to account for topographical relief. This result needs to be interpreted within the context of the inherent spatial and dimensional limitations of a 2D projection.

The microstructural and chemical data for the Ti/Nb nanolaminates with 3DIs provide key insights into the observed hardening effects when a triaxial stress state is applied perpendicular to the interfacial planes. The morphological characterization of the 3D 20-20 Ti/Nb sample, which contains relatively thicker 3DIs, reveals a subgranular morphology at the interface and a chemically tortuous interface as seen in Atom Probe Tomography (APT not shown) comprising a fraction of the total interfacial thickness. These nanoscale heterogeneities at the interface likely act as additional dislocation barriers, increasing resistance to dislocation motion and hindering slip transfer through the interface. The hardness data show higher hardness for thicker 3DIs, with all else being the same.

We can infer that when a complex stress state is applied perpendicular to the interface, this barrier effect is amplified due to the intricate interface morphology. Under uniaxial stress, dislocations may glide along a single plane, but a triaxial stress state introduces more complex shear and compressive components across the interface, potentially activating several mechanical hardening mechanisms simultaneously. In this case, dislocations must navigate a more tortuous path through the interfacial region, which increases the energy required for transmission. Our next step will be to apply loads in uniaxial compression and in shear to better understand the specific effects observed here. It is evident that the interface acts as a discontinuity in slip planes, preventing straightforward dislocation glide. The thicker the interface, the more heterogeneities and complex structures are present, further impeding dislocation motion.

The nanomechanical testing of the Ti/Nb nanolaminates demonstrates a clear correlation between 3DI thickness and material hardness. This can be seen in Fig. 5. The 3D 20-20 Ti/Nb sample exhibits a hardness of 5.8 GPa, while 3D 5-20 Ti/Nb sample has a hardness of 4.8 GPa. For the 3D 5-20 sample, the standard deviation in hardness was 0.039 GPa and the standard deviation in modulus was 0.887 GPa. For the 3D 20-20 sample, the standard deviation in hardness was 0.139 GPa, and the standard deviation in modulus was 1.260 GPa. These results suggest that thicker 3DIs significantly strengthen the material. The BCC Ti/Nb alloy film lacks well-defined layers and has no interfaces, shows a much lower hardness of 2.8 GPa suggesting a microstructure dependent strengthening. Our control is pure nanograined polycrystalline Ti to show that 3DIs are indeed causing a length scale dependent mechanical change, as opposed to the BCC Ti/Nb alloy, or an inherent effect from nanograined Ti. The increase in hardness with thicker interfaces is consistent with the PFDD model showing thicker 3DIs increase the critical stress required for dislocation glide through the interface. The observed strengthening effect in the nanolaminates show that thicker 3DIs serve as barriers to

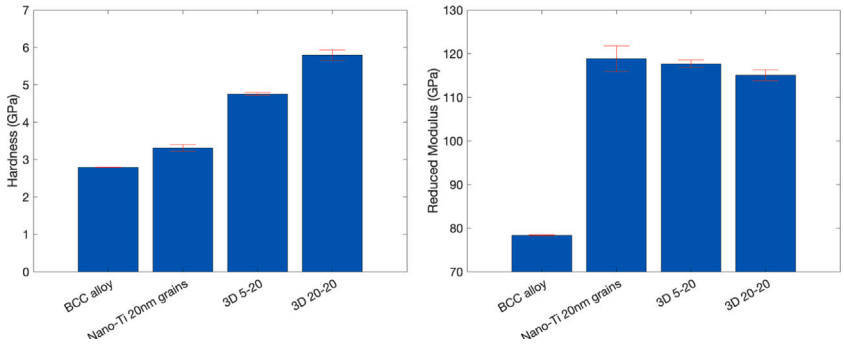

Fig. 5. Nanoindentation hardness (a) and reduced modulus (b).

dislocation motion and promote stronger resistance to slip transfer. Given that the processing of these 3DIs is quite challenging and time-intensive, computational efforts can aid to identify the extent to which thickening the 3D interface is beneficial.

The reduced modulus values across the Ti/Nb nanolaminate samples remain relatively stable and correspond to a rule-of-mixtures of 50% Ti, 50% Nb by volume, regardless of 3DI thickness. This stability suggests that the modulus is primarily governed by the inherent elastic properties of the constituent materials (Ti and Nb), rather than by the interface morphology. The reduced modulus measures the material elastic response, and for these materials, the elastic properties of both Ti and Nb remain stable across different length scales, unaffected by the introduction of 3DIs. An interesting observation is that the elimination of the nanolaminate structure, as seen in the BCC Ti/Nb alloy film, reduces the elastic robustness of the system. This reduction in modulus implies that the overall structure, rather than interfacial morphology, governs the elastic properties of the Ti/Nb nanolaminates. The nano-Ti sample, consisting of polycrystalline Ti without Nb or a nanolaminate structure, exhibits a similar reduced modulus to the Ti/Nb nanolaminates, indicating that the modulus is largely driven by the bulk properties of the Ti matrix, particularly its elastic constants. The presence of Nb layers and the introduction of 3DIs primarily influence the plastic response of the composite rather than its elastic properties. The elastic properties of Ti remain unchanged potentially due to the structural support provided by the nanolaminate architecture. The limited impact of the interfaces on the reduced modulus suggests that while 3DI morphology affects dislocation behavior (and thus hardness), it has little influence on the material's ability to deform elastically. The nano-Ti sample further supports this observation, as even without Nb or a nanolaminate structure, it exhibits similar reduced modulus values to the Ti/Nb nanolaminate samples. Thus, the elastic response is largely dependent on the stiffness of the Ti matrix itself when the nanolaminate structure is present, rather than on the interfacial structures or the introduction of 3DIs.

3.2. Ti-Nb binary properties

Fig. 2 shows the GSFE curve for the BCC Ti–Nb binary. The USFE ranges tightly around an average value of 458.97 mJ/m^2. For comparison, the Nb GSFE curve from a prior DFT calculation is shown. The USFE values of the Ti–Nb alloy are far lower, with a difference of $\Delta\gamma = 217.81 mJ/m^2$. Table 1 includes the elastic constants and lattice parameter from this calculation. The corresponding lattice constant is 3.287 nm, indicating a 0.55% lattice mismatch with Nb. All three cubic elastic constants are lower than those of Nb.

To quickly compare their moduli among materials with differing degrees of elastic anisotropy, the directional shear moduli μ_{dir} in the plane of glide are estimated by transforming the elastic tensor accordingly and then applying the Voigt approximation. μ_{dir} is provided in Table 1. Compared to the BCC phases, the μ_{dir} and USFE values in Ti are much lower, which would suggest a preference for the dislocation to be in the Ti phase as opposed to the other phases.

3.3. Lattice glide stresses

We first estimate τ_0, a critical stress for glide of an edge dislocation in a given glide plane in either Ti or Nb alone free of other phases. These critical glide stresses will serve as reference stresses to aid comparisons across materials and systems and to help elucidate the obstacle effect of the 3DI. First, the relaxed dislocation core structure under zero stress is determined. For both Ti and Nb, edge dislocations achieve a planar, narrow core of finite width. Next, for τ_0, we determine the minimum applied shear stress to initiate its motion in a large crystal, free of interfaces. (Variously also called a lattice friction stress or a Peierls stress.) When expressed in μ_{Nb}, effective isotropic modulus of Nb, τ_0 are calculated to be $0.0335\mu_{Nb}$, $0.0066\mu_{Nb}$, and $0.0054\mu_{Nb}$ for the {110} Nb plane, and for the prismatic and basal Ti planes, respectively. Considering these calculations are for undissociated dislocations and lack finite temperature effects, their values are expected to be relatively high.

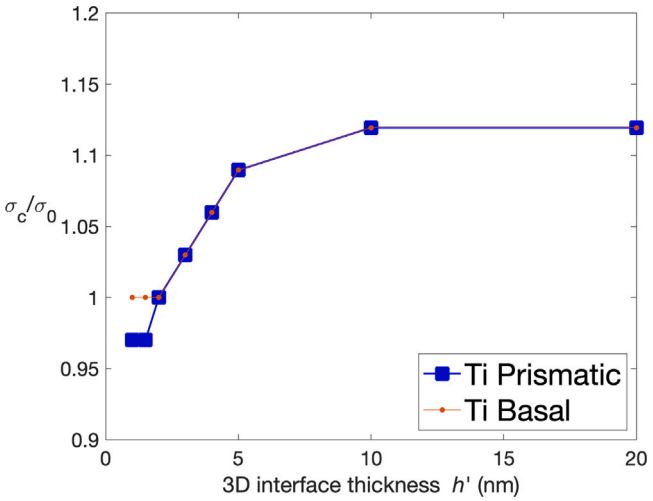

Fig. 6. Normalized critical stresses for an edge dislocation as a function of 3DI thickness starting in Nb and moving into Ti basal (red) and Ti prismatic (blue). (For interpretation of the references to color in this figure legend, the reader is referred to the web version of this article.)

3.4. Critical slip transfer stresses

Fig. 6 examines the effect h' on τ_c required to transfer a Nb dislocation across the 3DI into Ti via either the Prismatic or Basal pathway. To elucidate the strengthening potential, we plot the ratio $\bar{\tau}_c = \tau_c/\tau_0$. When crossing into the Ti prismatic plane over the 2D interface ($h' = 1$ nm), $\bar{\tau}_c = \tau_c/\tau_0$ is less than unity. The interface poses no barrier and in fact it is easier for the dislocation to glide in Ti than in Nb. When the transfer takes place along the Nb to basal plane pathway, $\bar{\tau}_c = \tau_c/\tau_0$ is unity. In essence, the Nb dislocation glides across the interface unhindered. The ease for which this slip transfer happens is expected, by taking into consideration the reduction in μ_{dir} and USFE when transferring from Nb to Ti on either plane. It should be noted that a residual dislocation forms in the interface, but evidently the associated energetic penalty is not sufficient to pose a barrier.

When the interface thickness increases to $h' = 2$ nm or greater, a sufficient amount of atomic planes has been introduced to define a 3DI. For $h' = 2$ nm alone, $\bar{\tau}_c$ for both the prismatic and basal slip pathways become unity. A stress sufficient to glide in Nb is sufficient to glide across a $h' = 2$ nm thick interface. This fine 3D Ti–Nb layer has removed the orientation dependence between these two pathways, as well as maintained the glide resistance of the dislocation in Nb, even though the dislocation is transferring to a material with a lower glide resistance.

Importantly, as h' increases from 2 nm to 10 nm, $\bar{\tau}_c$ increases. This positive size effect is seen for both slip pathways. Thicker interfaces are stronger interfaces up until a certain point, where the elastic image effects are no longer prevalent.

We next examine the slip transfer in the reverse direction, from Ti to Nb. Fig. 7 shows the calculated $\bar{\tau}_c$ for either Ti prismatic or basal dislocations to cross the interface and glide into Nb. A 2D interface ($h' = 1$ nm) poses a slip resistance that is over three times that to induce glide in Ti alone. The interface resistance is attributed to the motion of the dislocation from a more compliant, lower USFE Ti phase into Nb, which is stiffer and possesses a USFE that is nearly two or three times greater. Based on analytical arguments for elastic and stacking fault effects, this interfacial resistance is expected.

Thickening the interface $h' > 1$ nm causes marked increases in $\bar{\tau}_c$. The slip resistance increases up to eight times for prismatic dislocations and over 10 times for basal dislocations. Like the reverse path from Nb to Ti, $\bar{\tau}_c$ increases as h' increases up to about $h' = 10$ nm, beyond which the increments in $\bar{\tau}_c$ become smaller. The highest $\bar{\tau}_c$ is reached for $h' = 20$ nm, only because it is the thickest interface we studied. Unlike the reverse path, however, the positive size effect of h' is much more profound. With all else being the same, thicker interfaces are stronger interfaces for the Ti to Nb transfer direction as well.

3DIs more effectively strengthen the composite when Ti dislocations transfer to Nb than vice versa. It is therefore possible that a 3DI can switch the slip transfer asymmetry of the 2D interface. Fig. 8 plots the change in the asymmetry ratio, the slip transfer stress for Nb to Ti to that for the reverse direction, with increasing 3D h'. For sharp interfaces ($h' = 1$ nm), the ratio is greater than unity but as $h' > 2$ nm, the ratio reduces below unity, signifying that transfer of Ti dislocations to Nb becomes the harder slip direction. Notably, the asymmetry is nearly removed for $h' = 2$ nm. The presence of a fine, few nm thick interface ($h' = 2$ nm) has resulted in direction-independent slip transfer between two metals with large differences in their crystal structure, USFE and elastic moduli. This may have implications for increased codeformation of Ti and Nb, which could contribute to increasing the elongation to failure. It may prevent localization and pile up predominantly in one phase more than the other. It could aid in achieving more isotropic deformation. Hence, it is likely that the 3DI thickness is one of the main parameters that dictates many more mechanical properties than just its strength.

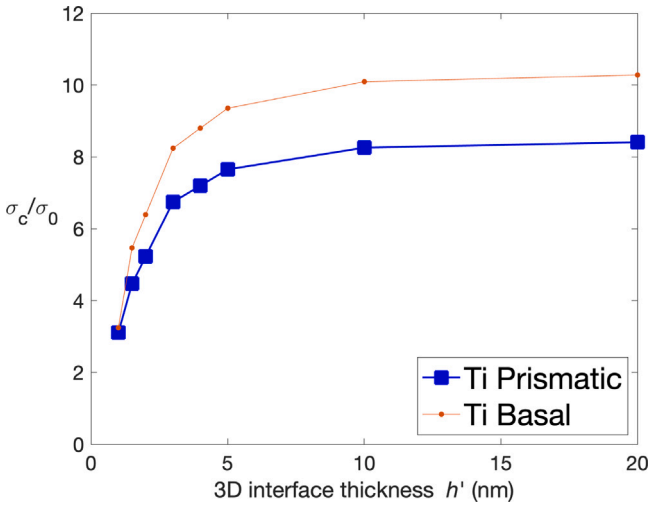

Fig. 7. Normalized critical stresses for an edge dislocation as a function of 3DI thickness starting in either Ti basal (red) or Ti prismatic (blue) and moving into Nb. (For interpretation of the references to color in this figure legend, the reader is referred to the web version of this article.)

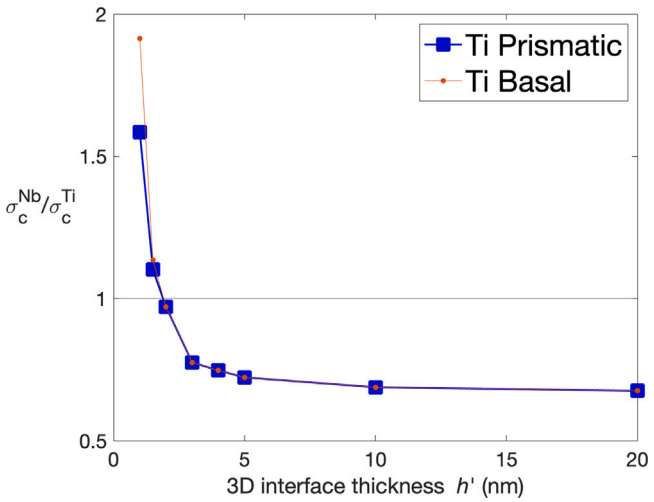

Fig. 8. Asymmetry ratio—the ratio of the critical stress for slip transfer for dislocations starting in Nb to dislocations starting in Ti on the basal plane (red) and prismatic plane (blue), respectively. (For interpretation of the references to color in this figure legend, the reader is referred to the web version of this article.)

3.5. Effect of material differences across the interface

When a dislocation glides across a boundary, three main property changes can affect the stress required: USFE, shear modulus and lattice parameter. The simulations for the slip transfer pathways to/from HCP Ti and BCC Nb, studied here account for all three. Their influences are coupled but among them, we observed that the influence of the USFE change is the most substantial. We can consider the analytical model by Zeng et al. (Eq. (2)) to help isolate the influence of the changes in lattice parameter and moduli, for which we use the directional shear modulus μ_{dir} (Zeng et al., 2016). For transfer across sharp Nb/Tibasal and Nb/Tiprismatic interfaces, the stress is two to three times higher than that for the reverse Ti basal/Nb and Ti prismatic/Nb. While quantitatively, the analytical model overestimates those critical stress values predicted by PFDD, the difference between the two orientations and pathways agree remarkably well. The differences in a and μ_{dir} dictate the critical stress for sharp interfaces.

When introducing the 3DI, two boundaries are created, e.g., one to cross Nb/3DI and the second to cross 3DI/Ti. The model can be applied to calculate the critical stress to cross each one. The critical stress to completely transfer across the entire 3DI is then taken as the higher stress of the two. With this approach, the model forecasts that the introduction of the 3DI results in a reduction in slip transfer stress from that of the 2D interface. This prediction disagrees with the calculations from PFDD, which clearly reveal an increase in slip transfer stress. The implication is that the strengthening results primarily from the changes in the USFE, which the analytical model (Eq. (2)) neglects.

4. Discussion

Experiments on Ti/Nb nanolaminates observe an increase in hardness with introduction of a 3DI and with increasing h'. The simulations performed here aim to isolate the effect of a 3DI on the stress required for a dislocation to glide across it. The calculation shows that 3DIs hinder dislocation transfer to/from the Ti and Nb layer compared to 2D interfaces and can contribute to the higher hardness in the 3DI-containing nanolaminate. They further forecast that resistance for slip transfer in both directions increases as h' to approximately 5–10 nm. This range is relatively broad when compared to the core of the dislocation (≈1 nm) and typical layer thicknesses in nanolaminates (≈ 10 nm to 100 nm). Analysis points to the interaction of the elastic fields of the dislocation with those arising from the elastic mismatch among the different phases as the origin of the size effect.

In their individual ways, both the elastic moduli mismatch and USFE mismatch contribute to the critical stress for slip transfer and in a fashion as that predicted by Koehler and Hirsch and Kelly (Koehler, 1970; Hirsch and Kelly, 1965), i.e., the greater their differences, the greater the hindrance to glide. Beyond 10 nm, the strengthening potential plateaus. To harness the gains, the 3DI only needs to be ”thick enough”; therefore, precise control of 3DI thickness is not needed. We can further speculate that undulating or variable thickness 3DIs of sufficient thickness ($h' > 3$ nm) will not lead to heterogeneity in slip transfer stress.

It could be argued that 3DIs are a mechanism to strengthen a nanolaminate, which already is an ultra-strong material. As in most cases, the pitfall of most ultra-high strength materials is the concomitant reduction in the strain-to-failure or ductility. The failure process, however, can be delocalized when the two materials of the nanolaminates are engineered to co-deform (Mayeur et al., 2015; Carpenter et al., 2015b; Misra et al., 2021). Minimizing or removing the asymmetry between the critical stresses for the two slip transfers directions can promote co-deformation. One of the more significant implications of the present work is that thickening the interface from 2D to 3D can not only strengthen, but also enable co-deformation between the pure phases. Prior works have successfully demonstrated that in some cases phase boundaries can help to overcome the strength-ductility trade-off (An et al., 2023; Yang et al., 2023). Since 3DIs are a type of phase boundary, we can expect that they hold the potential to break the strength-ductility trade-off as well. However, since 3DIs have a very different chemistry and structure than any phase boundaries that have been studied previously, their potential has yet to be clarified. 3DIs introduce many more tunable variables, like a characteristic thickness and composition variations, and the extent to which these details can strengthen (or weaken) the material is unknown.

Micropillar testing of various nanolaminates, e.g., Mg/Nb, Cu/Nb and even Cu/Nb with 3DIs, of different loading orientations have shown that their macroscopic strengths and deformation responses are anisotropic (Cheng et al., 2024; Jain et al., 2023; Li et al., 2012; Nizolek et al., 2016). For the Ti/Nb system, such tests have yet to be conducted. But regarding properties, anisotropy in this nanolaminate system lies at many levels. Both Nb and Ti are more elastically anisotropic compared to other pure BCC and HCP metals, Ti is plastically anisotropic, the crystals spanning the layers are highly oriented, there are different possible interfacial crystallographic characters, and the 2D layering has a single orientation. Accounting for these anisotropies, the model simulates slip transfer for two slip paths associated with two of the interfacial crystallographic characters. The 3DI preserves the anisotropies in slip transmission between these two orientations of the 2D interface. There is therefore no indication that a 3DI in the Ti/Nb system would diminish the strength anisotropy seen in the traditional Ti/Nb nanolaminate. Similar strength anisotropies between the 2D and 3D Cu/Nb systems was indeed seen in Cheng et al. (2024). In light of this, finding ways to overcome strength anisotropy while retaining the benefits of 3DIs are worthwhile. This notion is a similar goal to that of hierarchical materials, comprising nanolaminated grains that are randomly oriented throughout the microstructure (Zhang et al., 2019).

While there is experimental evidence of slip transmission of dislocations across a grain boundary (Lee et al., 1990), an analogous event across a phase boundary has not been reported in the literature to the authors' knowledge. However, slip band transfer across phase boundaries has been observed in nanolaminate systems, such as in Zheng et al. (2014), Zhang et al. (2019). A slip band represents the transmission of hundreds of dislocations. Slip band transfer is less difficult to capture since slip bands are higher length scale defects and hence easier to detect postmortem.

The 3DI is modeled here as a binary Ti–Nb solid solution BCC crystal. Although confirmation of its crystallinity awaits characterization, the Ti–Nb phase diagram indicates that this interface should be crystalline and most likely with a BCC structure for a broad range of Ti–Nb compositions, even for Ti-rich regions (with less than 5% Nb). The net composition of the entire 3DI is 50-50 Ti/Nb. Thus, we presume a homogeneous model 50/50 BCC interface was a reasonable representation of the chemistry and structure of the interface and in turn of the barrier strength against dislocation glide. However, it has been seen experimentally and can easily be anticipated as well that the 3DI will not be as homogeneous as modeled, but rather possess through-thickness composition and structure heterogeneities that depend on 3DI thickness. For instance, the gradients in the crystal structure and chemical composition could involve Ti-rich HCP portions of the interface bordering the Ti side and Nb-rich BCC portions on the Nb side and 50/50 BCC Ti–Nb in the center. The present model can easily incorporate such variations across the interface and the associated changes in stacking fault energy and elastic constants. However, obtaining an understanding of size effects alone would be obscured if all possible gradients through the thickness of the interface were introduced. At least to first order, the findings here can provide insight into thickness effects. The addition of the gradient may lead to slightly different size effects and strengthening behavior from those presented here, since the net changes transitions in elastic constants and stacking fault energies between the pure layers and the 3DIs will be the same.

One assumption that was made in the model was to neglect the effect of misfit dislocations that may be present. One of the motives of introducing a 3D interface is to remove the discrete misfit dislocation network. We do not expect a discrete set of misfit dislocations to be present in the 3D interface. If they were, the likely places would lie at the borders between either pure layer and the 3D interface. For a conservative estimate, we can consider the lattice misfit between the Nb region and the 3DI, there is a 1.11% misfit, implying that the interface will be nearly coherent. Between the Ti pure layer and the 3DI, the misfit lies between a

BCC phase and an HCP phase, which implies a semicoherent interface. Yet still the region near the Ti layer may be HCP, removing the need for misfit dislocations . At some distance from this border the 3D interface structure will give way to a BCC structure. Moreover, if a low density of misfits should exist, they would not vary with increasing 3DI thickness. The trend in critical slip transfer stress will be the same.

Future experiments could involve processing and testing samples with a range of 3DI thicknesses to determine whether the strengthening effect indeed plateaus at larger 3DI thicknesses. Care would need to be taken to maintain the same 3DI interface volume fraction.

Future simulations could investigate introducing a gradient interface, now that there is a baseline for the size effect due to the 3DI thickness. Furthermore, investigation of the effect of the pure layer thickness could be of interest.

The dislocations in simulation are compact and undissociated. While a good approximation for edge dislocations in Nb and basal dislocations in Ti, it may not be representative of prismatic dislocations in Ti. Prior modeling and experimental work have indicated that prismatic dislocations can split into two partials and separate by 0.5 nm (Albrecht et al., 2020). While this core width may appear narrow, it is possible that the leading and trailing partials can traverse the 3DI sequentially. Prior PFDD work on the full FCC nanolaminates with FCC 3DIs suggests that transfer of dissociated Cu dislocations can further enhance the 3DI thickness effect on slip transfer, when the core width is greater than the 3DI thickness. The model formulation can allow for dissociated dislocations and this is reasonable to include in future work to probe whether similar outcomes occur in nanolaminate systems involving well extended dislocations. However in the present case, the cores in Ti and Nb are expected to be far narrower than the 3DI thicknesses we consider. Here indeed, the focus lies in isolating the contribution of 3DI size effects, which we see is significant for thicknesses much larger the core width of the transmitting dislocations.

5. Conclusions

In this work we study an HCP/BCC Ti/Nb nanolaminate system with 3D ”thick” biphase interfaces in Ti/Nb nanolaminates. Initial experimental hardness tests suggest that thicker 3DI increases strength. Specifically it is shown that when the 3DI thickness increases from h’= 5 to 20 nm, while keeping the layer thicknesses approximately the same, the hardness increases. To probe possible mechanisms, we develop a phase-field dislocation dynamics (PFDD) model for dislocation glide in a multi-phase hexagonal close packed and body centered cubic system. The model is applied to simulate the slip transfer of dislocations across both sharp 2D and thick 3D biphase interfaces in Ti/Nb nanolaminates. The computational results show that thick 3DIs can increase the critical stress to fully transfer across the interface to/from Ti and Nb compared that for a sharp 2D. Notably, the 3DI size effect is positive. That is, the critical slip transfer stress increases as 3DI thickness increases from 2 to 10 nm and plateaus thereafter. The model further suggests that introduction of a 3DI of a special thickness (2 nm in the present system) can minimize or even eliminate the asymmetry in slip transfer.

CRediT authorship contribution statement

Nicolas Fuchs-Lynch: Writing – original draft, Visualization, Investigation, Formal analysis. **Mauricio De Leo:** Writing – review & editing, Investigation. **Pulkit Garg:** Investigation. **Shuozhi Xu:** Software, Methodology. **Nathan A. Mara:** Writing – review & editing, Supervision. **Irene J. Beyerlein:** Writing – review & editing, Supervision, Methodology, Conceptualization.

Declaration of competing interest

The authors declare that they have no known competing financial interests or personal relationships that could have appeared to influence the work in this paper.

Acknowledgments

The authors acknowledge financial support from the Department of Energy, Office of Science, Basic Energy Sciences Program DE-SC0020133. Use was made of computational facilities purchased with funds from the National Science Foundation, United States (CNS-1725797) and administered by the Center for Scientific Computing (CSC). The CSC is supported by the California NanoSystems Institute and the Materials Research Science and Engineering Center (MRSEC; NSF DMR 2308708) at UC Santa Barbara. Access to the University of Minnesota’s Characterization Facility for FIB/SEM, TEM and nanoindentation testing is gratefully acknowledged. This work was performed, in part, at the Center for Integrated Nanotechnologies, an Office of Science User Facility operated for the U.S. Department of Energy (DOE) Office of Science by Los Alamos National Laboratory (Contract 89233218CNA000001) and Sandia National Laboratories (Contract DE-NA-0003525).

Appendix A. Supplementary data

Supplementary material related to this article can be found online at https://doi.org/10.1016/j.ijplas.2025.104246.

Data availability

Data will be made available on request.

References

Acharya, A., 2007. Jump condition for GND evolution as a constraint on slip transmission at grain boundaries. Phil. Mag. 87 (8–9), 1349–1359.

Agius, D., Kareer, A., Al Mamun, A., Truman, C., Collins, D.M., Mostafavi, M., Knowles, D., 2022. A crystal plasticity model that accounts for grain size effects and slip system interactions on the deformation of austenitic stainless steels. Int. J. Plast. 152, 103249.

Ahmadikia, B., Kumar, M.A., Beyerlein, I.J., 2021. Effect of neighboring grain orientation on strain localization in slip bands in HCP materials. Int. J. Plast. 144, 103026.

Albiez, J., Erdle, H., Weygand, D., Böhlke, T., 2019. A gradient plasticity creep model accounting for slip transfer/activation at interfaces evaluated for the intermetallic NiAl-9Mo. Int. J. Plast. 113, 291–311.

Albrecht, C., Hunter, A., Kumar, A., Beyerlein, I.J., 2020. A phase field model for dislocations in hexagonal close packed crystals. J. Mech. Phys. Solids 137, 103823.

An, Z., Mao, S., Liu, Y., Yang, L., Vayyala, A., Wei, X., Liu, C., Shi, C., Jin, H., Liu, C., et al., 2023. Inherent and multiple strain hardening imparting synergistic ultrahigh strength and ductility in a low stacking faulted heterogeneous high-entropy alloy. Acta Mater. 243, 118516.

Ashmawi, W., Zikry, M., 2002. Prediction of grain-boundary interfacial mechanisms in polycrystalline materials. J. Eng. Mater. Technol. 124 (1), 88–96.

Beyerlein, I., Demkowicz, M., Misra, A., Uberuaga, B., 2015. Defect-interface interactions. Prog. Mater. Sci. 74, 125–210.

Beyerlein, I.J., Hunter, A., 2016. Understanding dislocation mechanics at the mesoscale using phase field dislocation dynamics. Phil. Trans. R. Soc. A 374 (2066), 20150166.

Beyerlein, I.J., Li, Z., Mara, N.A., 2022. Mechanical properties of metal nanolaminates. Annu. Rev. Mater. Res. 52 (1), 281–304.

Beyerlein, I.J., Mayeur, J.R., 2015. Mesoscale investigations for the evolution of interfaces in plasticity. Curr. Opin. Solid State Mater. Sci. 19 (4), 203–211.

Beyerlein, I.J., Wang, J., 2019. Interface-driven mechanisms in cubic/noncubic nanolaminates at different scales. MRS Bull. 44 (1), 31–39.

Bönisch, M., 2016. Structural Properties, Deformation Behavior and Thermal Stability of Martensitic Ti-Nb Alloys (Ph.D. thesis). Technische Univ. Dresden (Germany). Fakultaet fuer Mathematik und Naturwissenschaften.

Bormann, F., Peerlings, R.H., Geers, M.G., Svendsen, B., 2019. A computational approach towards modelling dislocation transmission across phase boundaries. Phil. Mag..

Campbell, J.E., Goodwin, H., Wagner, H., Douglass, R., Allen, B., 1961. Introduction to Metals for Elevated-Temperature Use. vol. 160, Defense Metals Information Center, Battelle Memorial Institute.

Cantwell, P.R., Frolov, T., Rupert, T.J., Krause, A.R., Marvel, C.J., Rohrer, G.S., Rickman, J.M., Harmer, M.P., 2020. Grain boundary complexion transitions. Annu. Rev. Mater. Res. 50 (1), 465–492.

Carpenter, J.S., Nizolek, T., Mccabe, R.J., Knezevic, M., Zheng, S., Eftink, B.P., Scott, J.E., Vogel, S.C., Pollock, T.M., Mara, N.A., et al., 2015a. Bulk texture evolution of nanolamellar Zr–Nb composites processed via accumulative roll bonding. Acta Mater. 92, 97–108.

Carpenter, J., Nizolek, T., McCabe, R., Zheng, S., Scott, J., Vogel, S., Mara, N., Pollock, T., Beyerlein, I.J., 2015b. The suppression of instabilities via biphase interfaces during bulk fabrication of nanograined Zr. Mater. Res. Lett. 3 (1), 50–57.

Chen, Y., Li, N., Hoagland, R.G., Liu, X.-Y., Baldwin, J., Beyerlein, I.J., Cheng, J., Mara, N., 2020a. Effects of three-dimensional Cu/Nb interfaces on strengthening and shear banding in nanoscale metallic multilayers. Acta Mater. 199, 593–601.

Chen, Y., Shao, S., Liu, X.-Y., Yadav, S.K., Li, N., Mara, N., Wang, J., 2017. Misfit dislocation patterns of Mg-Nb interfaces. Acta Mater. 126, 552–563.

Chen, T., Yuan, R., Beyerlein, I.J., Zhou, C., 2020b. Predicting the size scaling in strength of nanolayered materials by a discrete slip crystal plasticity model. Int. J. Plast. 124, 247–260.

Cheng, J.Y., Wang, J., Chen, Y., Xu, S., Barriocanal, J.G., Baldwin, J.K., Beyerlein, I.J., Mara, N.A., 2024. 3D interfaces enhance nanolaminate strength and deformability in multiple loading orientations. Acta Mater. 267, 119697.

Cheng, J.Y., Xu, S., Chen, Y., Li, Z., Baldwin, J.K., Beyerlein, I.J., Mara, N.A., 2022. Simultaneous high-strength and deformable nanolaminates with thick biphase interfaces. Nano Lett. 22 (5), 1897–1904.

Demkowicz, M.J., Wang, J., Hoagland, R.G., 2008. Interfaces between dissimilar crystalline solids. In: Dislocations in Solids. Vol. 14, Elsevier, pp. 141–205.

Eshelby, J.D., 1957. The determination of the elastic field of an ellipsoidal inclusion, and related problems. Proc. R. Soc. Lond. Ser. A. Math. Phys. Sci. 241 (1226), 376–396.

Fey, L.T., Hunter, A., Beyerlein, I.J., 2022. Phase-field dislocation modeling of cross-slip. J. Mater. Sci. 1–15.

Graff, S., 2008. Micromechanical Modeling of the Deformation of HCP Metals (Ph.D. thesis). GKSS-Forschungszentrum Geesthacht GmbH (Germany). Inst. fuer Materialforschung.

Haouala, S., Alizadeh, R., Bieler, T., Segurado, J., LLorca, J., 2020. Effect of slip transmission at grain boundaries in Al bicrystals. Int. J. Plast. 126, 102600.

Hasirci, V., Hasirci, N., 2018. Fundamentals of Biomaterials. Springer.

Hirsch, P.B., Kelly, A., 1965. Stacking-fault strengthening. Philos. Magazine: A J. Theor. Exp. Appl. Phys. 12 (119), 881–900.

Holec, D., Friák, M., Neugebauer, J., Mayrhofer, P.H., 2012. Trends in the elastic response of binary early transition metal nitrides. Phys. Rev. B— Condens. Matter Mater. Phys. 85 (6), 064101.

Hunter, A., Leu, B., Beyerlein, I.J., 2018. A review of slip transfer: applications of mesoscale techniques. J. Mater. Sci. 53, 5584–5603.

Jain, M., Yaddanapudi, K., Kidigannappa, A.T., Baldwin, K., Knezevic, M., Mara, N.A., Beyerlein, I.J., Pathak, S., 2023. Simultaneous high strength and mechanical stability of bcc Nb/Mg nanolaminates. Acta Mater. 242, 118487.

Jian, W.-R., Su, Y., Xu, S., Ji, W., Beyerlein, I.J., 2021. Effect of interface structure on dislocation glide behavior in nanolaminates. J. Mater. Res. 36 (13), 2802–2815.

Khalajhedayati, A., Rupert, T.J., 2015. High-temperature stability and grain boundary complexion formation in a nanocrystalline Cu-Zr alloy. Jom 67, 2788–2801.

Koehler, J., 1970. Attempt to design a strong solid. Phys. Rev. B 2 (2), 547.

Lee, T., Robertson, I., Birnbaum, H., 1990. TEM in situ deformation study of the interaction of lattice dislocations with grain boundaries in metals. Phil. Mag. A 62 (1), 131–153.

Lei, L., Marin, J.L., Koslowski, M., 2013. Phase-field modeling of defect nucleation and propagation in domains with material inhomogeneities. Modelling Simul. Mater. Sci. Eng. 21 (2), 025009.

Li, N., Mara, N., Wang, J., Dickerson, P., Huang, J., Misra, A., 2012. Ex situ and in situ measurements of the shear strength of interfaces in metallic multilayers. Scr. Mater. 67 (5), 479–482.

Liang, F., Wang, Z.-X., Li, M.-Y., Zhang, B., Luo, X.-M., Zhu, X.-F., Zhang, G.-P., 2024. Exceptional ductility through interface-constrained grain growth for the ultrafine-scale Ni/Ni-W layered composites. Int. J. Plast. 176, 103959.

Liu, J.Z., Van De Walle, A., Ghosh, G., Asta, M., 2005. Structure, energetics, and mechanical stability of Fe-Cu bcc alloys from first-principles calculations. Phys. Rev. B— Condens. Matter Mater. Phys. 72 (14), 144109.

Mara, N.A., Beyerlein, I.J., 2014. Effect of bimetal interface structure on the mechanical behavior of Cu–Nb fcc–bcc nanolayered composites. J. Mater. Sci. 49, 6497–6516.
Mara, N., Bhattacharyya, D., Hirth, J., Dickerson, P., Misra, A., 2010. Mechanism for shear banding in nanolayered composites. Appl. Phys. Lett. 97 (2).
Martínez, E., Caro, A., Beyerlein, I.J., 2014. Atomistic modeling of defect-induced plasticity in CuNb nanocomposites. Phys. Rev. B 90 (5), 054103.
Mayeur, J., Beyerlein, I.J., Bronkhorst, C., Mourad, H., 2015. Incorporating interface affected zones into crystal plasticity. Int. J. Plast. 65, 206–225.
Mianroodi, J.R., Svendsen, B., 2015. Atomistically determined phase-field modeling of dislocation dissociation, stacking fault formation, dislocation slip, and reactions in fcc systems. J. Mech. Phys. Solids 77, 109–122.
Misra, A., Göken, M., Mara, N.A., Beyerlein, I.J., 2021. Hierarchical and heterogeneous multiphase metallic nanomaterials and laminates. MRS Bull. 46, 236–243.
Misra, A., Hirth, J., Kung, H., 2002. Single-dislocation-based strengthening mechanisms in nanoscale metallic multilayers. Phil. Mag. A 82 (16), 2935–2951.
Nasim, M., Li, Y., Wen, M., Wen, C., 2020. A review of high-strength nanolaminates and evaluation of their properties. J. Mater. Sci. Technol. 50, 215–244.
Nizolek, T., Beyerlein, I.J., Mara, N.A., Avallone, J.T., Pollock, T.M., 2016. Tensile behavior and flow stress anisotropy of accumulative roll bonded Cu-Nb nanolaminates. Appl. Phys. Lett. 108 (5).
Pathak, S., Velisavljevic, N., Baldwin, J.K., Jain, M., Zheng, S., Mara, N.A., Beyerlein, I.J., 2017. Strong, ductile, and thermally stable bcc-Mg nanolaminates. Sci. Rep. 7 (1), 8264.
Perdew, J.P., Burke, K., Ernzerhof, M., 1996. Generalized gradient approximation made simple. Phys. Rev. Lett. 77 (18), 3865.
Rao, S., Hazzledine, P., 2000. Atomistic simulations of dislocation–interface interactions in the Cu-Ni multilayer system. Phil. Mag. A 80 (9), 2011–2040.
Roach, A.M., Xu, S., Luscher, D.J., Gianola, D.S., Beyerlein, I.J., 2023. Interaction of extended dislocations with nanovoid clusters. Int. J. Plast. 168, 103684.
Rodney, D., Ventelon, L., Clouet, E., Pizzagalli, L., Willaime, F., 2017. Ab initio modeling of dislocation core properties in metals and semiconductors. Acta Mater. 124, 633–659.
Simmons, G., 1971. Single crystal elastic constants and caluculated aggregate properties. A Handb. 4.
Van De Walle, A., Asta, M., Ceder, G., 2002. The alloy theoretic automated toolkit: A user guide. Calphad 26 (4), 539–553.
Wang, Y., Li, J., 2010. Phase field modeling of defects and deformation. Acta Mater. 58 (4), 1212–1235.
Wang, J., Misra, A., 2011. An overview of interface-dominated deformation mechanisms in metallic multilayers. Curr. Opin. Solid State Mater. Sci. 15 (1), 20–28.
Wang, J., Zhang, R., Zhou, C., Beyerlein, I.J., Misra, A., 2014. Interface dislocation patterns and dislocation nucleation in face-centered-cubic and body-centered-cubic bicrystal interfaces. Int. J. Plast. 53, 40–55.
Warlimont, H., Martienssen, W., 2018. Springer Handbook of Materials Data. Springer.
Woo, C., 2000. Defect accumulation behaviour in hcp metals and alloys. J. Nucl. Mater. 276 (1–3), 90–103.
Wu, H., Huang, M., Xia, Y., Li, X., Li, R., Liu, C., Gan, W., Xiao, T., Geng, L., Liu, Q., et al., 2023. The importance of interfacial stress-affected zone in evading the strength-ductility trade-off of heterogeneous multi-layered composites. Int. J. Plast. 160, 103485.
Xu, S., Cheng, J.Y., Li, Z., Mara, N.A., Beyerlein, I.J., 2022a. Phase-field modeling of the interactions between an edge dislocation and an array of obstacles. Comput. Methods Appl. Mech. Engrg. 389, 114426.
Xu, S., Cheng, J.Y., Mara, N.A., Beyerlein, I.J., 2022b. Dislocation dynamics in heterogeneous nanostructured materials. J. Mech. Phys. Solids 168, 105031. http://dx.doi.org/10.1016/j.jmps.2022.105031, URL https://www.sciencedirect.com/science/article/pii/S0022509622002083.
Xu, S., Cheng, J., Mara, N., Beyerlein, I.J., 2022c. Thick interface size effect on dislocation transmission in nanolaminates. In: IOP Conference Series: Materials Science and Engineering. Vol. 1249, IOP Publishing, 012005.
Xu, S., Hwang, E., Jian, W.-R., Su, Y., Beyerlein, I.J., 2020a. Atomistic calculations of the generalized stacking fault energies in two refractory multi-principal element alloys. Intermetallics 124, 106844.
Xu, S., Mianroodi, J.R., Hunter, A., Svendsen, B., Beyerlein, I.J., 2020b. Comparative modeling of the disregistry and Peierls stress for dissociated edge and screw dislocations in Al. Int. J. Plast. 129, 102689.
Xu, S., Smith, L., Mianroodi, J.R., Hunter, A., Svendsen, B., Beyerlein, I.J., 2019. A comparison of different continuum approaches in modeling mixed-type dislocations in Al. Modelling Simul. Mater. Sci. Eng. 27 (7), 074004.
Yang, C., Zhang, B., Fu, L., Wang, Z., Teng, J., Shao, R., Wu, Z., Chang, X., Ding, J., Wang, L., et al., 2023. Chemical inhomogeneity–induced profuse nanotwinning and phase transformation in AuCu nanowires. Nat. Commun. 14 (1), 5705.
Yu-Zhang, K., Embury, J., Han, K., Misra, A., 2008. Transmission electron microscopy investigation of the atomic structure of interfaces in nanoscale Cu–Nb multilayers. Phil. Mag. 88 (17), 2559–2567.
Zeng, Y., Cai, X., Koslowski, M., 2019. Effects of the stacking fault energy fluctuations on the strengthening of alloys. Acta Mater. 164, 1–11.
Zeng, Y., Hunter, A., Beyerlein, I.J., Koslowski, M., 2016. A phase field dislocation dynamics model for a bicrystal interface system: An investigation into dislocation slip transmission across cube-on-cube interfaces. Int. J. Plast. 79, 293–313.
Zhang, J.-W., Beyerlein, I.J., Han, W.-Z., 2019. Hierarchical 3D nanolayered duplex-phase Zr with high strength, strain hardening, and ductility. Phys. Rev. Lett. 122 (25), 255501.
Zheng, S., Wang, J., Carpenter, J., Mook, W., Dickerson, P., Mara, N., Beyerlein, I.J., 2014. Plastic instability mechanisms in bimetallic nanolayered composites. Acta Mater. 79, 282–291.